Journal of JSEM, Vol.12, Special Issue (2012) s198-s204
Copyright © 2012 JSEM

Dynamic Property Evaluation of PLLA/PBSL Polymer Blends using Compressive and Tensile Split Hopkinson Bar Methods

Seiya KUNO[1], Masahiro NISHIDA[1], Ikuyo KAWASHIMA[1], Tetsuo TAKAYAMA[2] and Mitsugu TODO[3]

[1] Graduate School of Engineering, Nagoya Institute of Technology, Gokiso-cho, Showa-ku, Aichi, 466-8555 Japan
[2] Graduate School of Science and Engineering, Yamagata University, 4-3-16 Jonan, Yonezawa,Yamagata, 992-8510, Japan
[3] Research Institute for Applied Mechanics, Kyushu University, 6-1 Kasuga-koen, Kasuga, Fukuoka, 816-8580, Japan

(*Received 17 January 2012; received in revised form 23 April 2012; accepted 26 April 2012*)

Abstract
The compressive and tensile properties of PLLA/PBSL polymer blends (90/10, 80/20, 70/30) were measured using a universal testing machine and split Hopkinson bar methods. The yield stress of static and dynamic compressive tests for the polymer blends decreased gradually with increasing PBSL. When PLLA/PBSL =100/0, 90/10 and 80/20, a wave-like shape such as Mackerel pattern were observed on the fracture surfaces of specimens after the static tensile tests. The fracture surfaces after the dynamic tensile tests were flat.

Key words
Poly(L-lactic acid), Poly (butylene succinate-co-L-lactate), Split Hopkinson Bar Method, Yield Stress, Fracture Surface Observation

1. Introduction

Poly(lactic acid) (PLLA) is a typical bio-based (plant-derived) and biodegradable polymer. It has been recognized as a promising alternative material for petroleum-based polymers. In order to overcome the brittleness and low impact strength of PLLA, its mechanical properties have been improved by blending with ductile polymers or natural fiber reinforcing.

Many attempts have been reported on the creation of polymer blends of PLLA and ductile polymers; for example, poly(ε-caprolactone) (PCL) [1-4], poly (butylene succinate) (PBS) [5-6], poly(butylene succinate-co-lactate) (PBSL) [4, 7-8] and Poly(butylene succinate-co-e-caprolactone) (PBSC) [9]. In the most cases the impact resistances of the polymer blends were evaluated by the Izod impact test/Charpy impact test and Dynatup impact test/dart impact test. Although good impact strengths have been reported, the basic mechanical properties with respect to impact resistances are still unknown. Also, these mechanical properties have not yet been fully elucidated at higher strain rates.

In the present study, the stress-strain curves of PLLA/PBSL polymer blend specimens were measured using compressive and tensile split Hopkinson bar (Kolsky bar) methods and using a universal testing machine. The effect of PBSL content on the stress-strain relations was discussed. The Young's modulus and yield stress measured by static compressive tests were compared with the theoretical modulus derived from the Halpin-Tsai model, Voigt model and Reuss model using the results of PLLA and PBSL. The fracture surface after static and dynamic tensile tests was observed in detail.

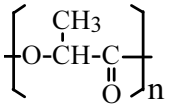

(a) PLLA

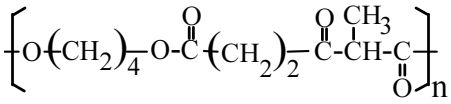

(b) PBSL

Fig. 1 Chemical structural formula of PLLA and PBSL

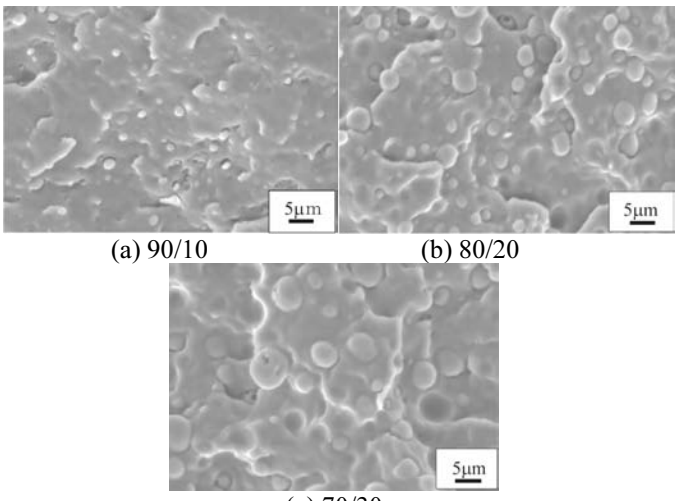

(a) 90/10 (b) 80/20

(c) 70/30

Fig. 2 Photographs of cryo-fractured surfaces taken using a scanning electron microscope

2. Materials

Polymer blends of PLLA and PBSL were prepared using PLLA from Shimadzu Co., Ltd. (Lacty® #5000) and PBSL from Mitsubishi Chemical Co. (GS Pla® AZ-Type, lactate unit ca. 3%). Because PBSL is a relatively new biodegradable polymer, there are many possibilities for high mechanical properties (for example, high impact strength) in polymer blends with PLLA.

The chemical structural formulas of PLLA and PBSL are shown in Fig. 1. The mixing ratios (mass fraction) of PLLA and PBSL were 90/10, 80/20, 70/30. After melt-mixing in a conventional melt-mixer at 190°C for 20 min and at a rotor speed of 50 rpm, the blend mixtures were press-processed using a conventional hot press at 190°C and 30 MPa for 30 min. Photographs of cryo-fractured surfaces using a scanning electron microscope (SEM, Hitachi S-3000NA) are shown in Fig. 2. Cryo-fracture surfaces were obtained by immersing the specimens in

liquid nitrogen for 3 min. PBSL spherical particles of 1 μm for PLLA/PBSL=90/10, 2-5 μm for 80/20 and 5-7 μm for 70/30 were dispersed, and a two-phase structure was observed. PBSL particle size became larger with increasing PBSL content.

Differential scanning calorimetry (DSC) thermograms of PLLA/PBSL blends are shown in Fig. 3 as well as the results of PLLA and PBSL. Dips near 172-173°C and 111-112°C showing the melting points of PLLA and PBSL were observed. The peaks near 85-100°C and dips near 60°C show the crystallization temperature and glass transition temperature of PLLA, respectively. However, the peak of glass transition temperature (about –33°C) of PBSL was not observed. Peaks of PLLA and PBSL independently appeared in the results of DSC thermograms. Phase separation of PLLA and PBSL could be confirmed by observation of fracture surfaces as well as by the results of the DSC thermograms.

3. Test Specimens and Experimental Setup

Compressive test specimens were made using a turning machine, and their end faces were polished and parallelized. Dynamic compressive test specimens with a diameter of 12 mm were used. The specimen thickness was 4.8 mm, so that dynamic stress equilibrium within specimens could be achieved using our equipment. In the quasi-static tests, based on ASTM D695-02a, specimens with a diameter of 8 mm and a thickness of 12 mm were mainly used.

Quasi-static compressive tests were conducted at a strain rate of 10^{-3} s^{-1} using a universal testing machine (A&D Co., Ltd., RTM-500). At high strain rates of 530 to 1300 s^{-1}, the compressive properties of the specimens were examined by the split Hopkinson pressure bar method. Input and output bars were made of an aluminum alloy (A2024-T4), and they had a diameter of 28 mm and respective lengths of 1900 mm and 1300 mm. Strain gages were placed on both sides of the input and output bars at distances of 950 mm and 300 mm from the specimen, respectively. (See [10] about the details of split Hopkinson pressure bar.) The stress and strain on the specimens were calculated from the strain on the bars using eqns. (1) and (2) [11, 12].

$$\varepsilon(t) = \frac{c_3}{L}\int_0^t \left[\varepsilon_I(t) - \varepsilon_R(t) - \varepsilon_T(t)\right] dt \qquad (1)$$

$$\sigma(t) = \frac{AE}{A_S}\varepsilon_T(t) \qquad (2)$$

Here, ε_I, ε_R and ε_T denote the axial strains induced in the input bar by the incident wave and reflective wave, and in the output bar by the transmitted wave, respectively. E and c_3 respectively denote the Young's modulus and elastic wave velocity in the input and output bars. L denotes the specimen thickness. A and A_S denote the cross-sectional areas of the input/output bars and specimens, respectively. We used brass strikers with a diameter of 20 mm and lengths of 220–310 mm. The specimens were maintained at a temperature of 23±2°C using silicone rubber heaters (Heatwell®, Kawai Electric Heater Co., Ltd.), each with a length of 60 mm. We preserved the specimens in a

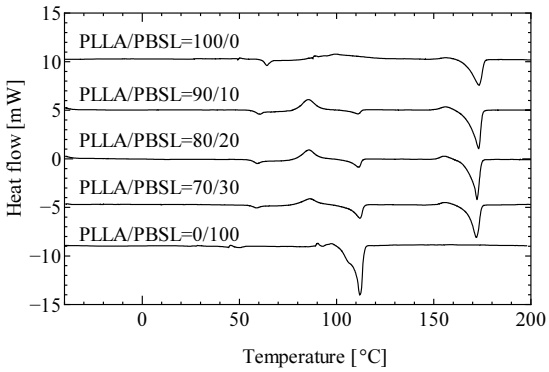

Fig. 3 Differential scanning calorimetry thermograms of PLLA/PBSL blends

Table 1 Melting points, crystallization temperature and glass transition temperature

PLLA/PBSL blend ratio	T_g of PLLA [°C]	T_c of PLLA [°C]	T_m of PBSL [°C]	T_m of PLLA [°C]
100/0	64.2	99.6	—	173.3
90/10	60.3	85.5	111.0	173.1
80/20	59.2	85.7	111.3	172.2
70/30	58.8	86.3	112.0	171.9
0/100	—	—	111.8	—

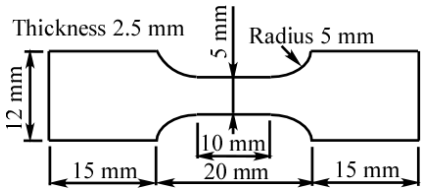

(a) Static test specimen

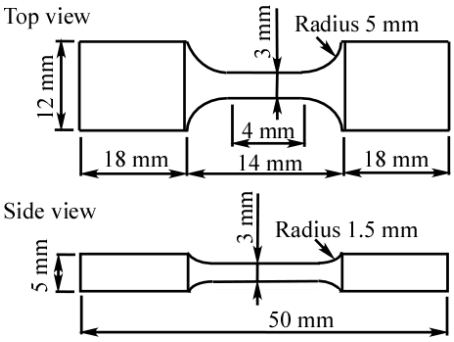

(b) Dynamic test specimen

Fig. 4 Specimen shape of tensile tests

Table 2 Material constants of input/output bars (Aluminum alloy A2024-T4 used in calculations)

	Density [kg/m^3]	Elastic wave velocity in bar, c_3 [m/s]	Young's modulus E [GPa]
Aluminum alloy A2024-T4	2.77×10^3	5150	73.6
Stainless steel SUS304	8.0×10^3	4970	200

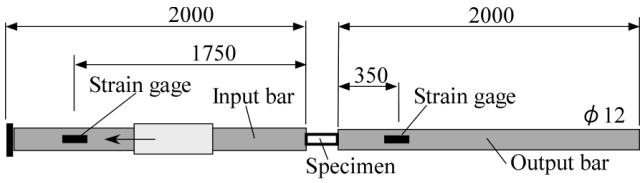

(a) Tensile split Hopkinson bar

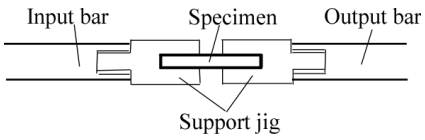

(b) Support jig of specimens

Fig. 5 Experimental setup for dynamic tensile tests

desiccator at a humidity of 30%–40% until just before use in order to avoid the effect of moisture absorption on the specimens. The material constants of the aluminum alloy (A2024-T4) bars used in the calculations are listed in Table 2.

Tensile test specimens were produced from the 5-mm-thick plates using a milling machine. In the case of static tests, a gage length region of approximately 5 mm × 2.5 mm and a gage length of 10 mm as shown in Fig. 4(a) were used. The quasi-static tests were conducted with a strain rate of 10^{-3} s^{-1}. The strain was calculated from the displacement of gage length using images taken by a camera. Dynamic tensile test specimens with a gage length region of approximately 3 mm × 3 mm and a gage length of 4 mm as shown in Fig. 4(b) were used. Because they are easy-to-make, plate-type specimens were employed. At high strain rates of 320 to 720 s^{-1}, the dynamic properties of the specimens were examined by the tensile split Hopkinson bar test in Fig. 5. The specimens were connected with input/output bars using support jigs. The strain on the specimens was calculated from the strain of the bars, as measured by the strain gages, using the following equations [11, 12]:

$$\varepsilon(t) = \frac{2c_3}{L_1}\int_0^t \left[\varepsilon_I(t) - \varepsilon_T(t)\right] dt \qquad (3)$$

Here, L_1 denotes the gage length. We used 4 mm as L_1 for sake of simplicity. The stress history of tensile tests was calculated from eq. (2). In fact, the tensile displacement using the tensile split Hopkinson bar method obtained by eq. (3) is not the displacement of gage length region. It is possible that the calculated strain includes the error caused by the deformation of shoulders part. The input and output bars were made of stainless steel (SUS304), and their material constants used in the calculations are listed in Table 2.

4. Results and Discussion

4.1 Static compressive tests

Fig. 6 shows the nominal stress–nominal strain curves in the low strain rate region obtained by the universal testing machine. The strain of specimens was calculated from the distance between compressive plates using an extensometer (Kyowa Electronic Instruments Co., Ltd., DTH-A). When PLLA/PBSL= 100/0 and 90/10, peaks of stress–strain curves was clearly observed. After the peak, strain softening was also seen on the curves When PLLA/PBSL=80/20 and 70/30, peaks of stress–strain curves were not clearly observed. In Table 3, yield stress decreased with increasing PBSL content. Here, when the peak of stress–strain curves was clearly observed, yield stress was defined as the peak stress near the elastic limit. Instead, when the peak of stress–strain curves was not observed, the yield stress was determined by the intersection of two asymptotic lines of elastic region and plastic region.

4.2 Dynamic compressive tests

Fig. 7 (a) and (b) show the nominal stress–nominal strain curves in the high strain rate region obtained by the split Hopkinson pressure bar method. Because the strain rate changed slightly during loadings, the average value of the strain rate–strain curve was used as the strain rate [13]. When PLLA/PBSL=100/0, just after stress–strain curve showed the maximum, the specimens were crushed and the stress decreased suddenly. When PLLA/PBSL=70/30 in addition to 90/10 and 80/20, strain softening was observed on the stress–strain curves. In the high strain region, yield stress also decreased with increasing PBSL content. Here, when the peak of stress–strain curves was clearly observed, yield stress was defined as the peak stress near the elastic limit. Instead, when the peak of stress–strain curves was not observed, the yield stress was determined by the intersection of two asymptotic lines of elastic region and plastic region.

4.3 Static tensile tests

Fig. 8 shows the nominal stress–nominal strain curves in the low strain rate region (1×10^{-4} s^{-1}) obtained by the universal testing machine. It seems that the specimens broke before showing a clear yield phenomenon. The initial slopes (Young's modulus) of PLLA/PBSL=100/0, 90/10, 80/20 and 70/30 were almost the same. Table 4 shows that the fracture strain of PLLA/PBSL=100/0, 90/10, 80/20 and 70/30 was also almost the same. The fracture strain of PLLA/PBSL= 100/0, 90/10, 80/20 and 70/30 was smaller than that of PLLA/PBSL=0/100. The tensile strength decreased gradually with increasing PBSL content. The tensile strength of PLLA/PBSL=70/30 was almost the same as that of PLLA/PBSL=0/100. Even though PBSL is ductile, the fracture strain for the polymer blends did not increase, as shown in Fig. 9 and Table 4.

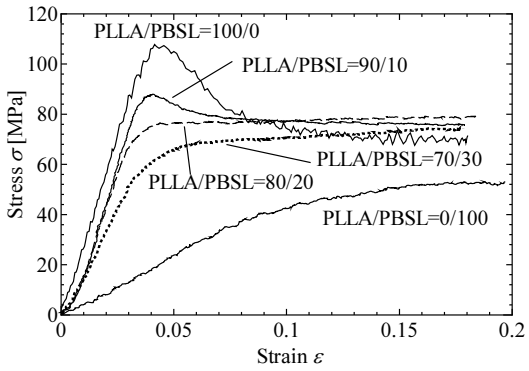

Fig. 6 Effect of PBSL content on compressive stress–strain curves at low strain rates (9.3×10^{-4} – 1.1×10^{-3} s^{-1})

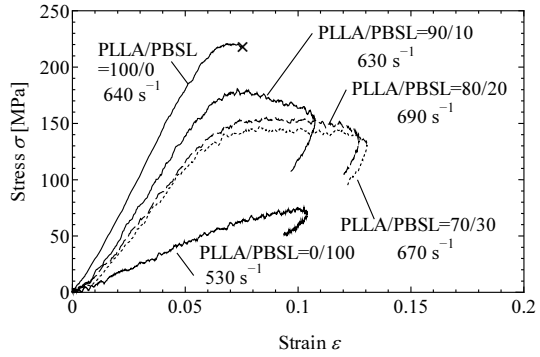

(a) Strain rates of 530-690 s^{-1}

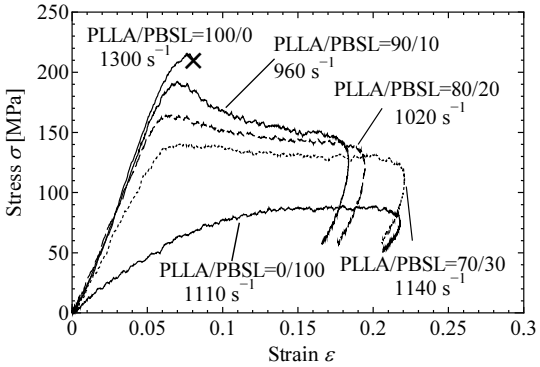

(b) Strain rates of 960-1300 s^{-1}

Fig. 7 Effect of PBSL content on compressive stress–strain curves at high strain rates

Table 3 Young's modulus and yield stress of PLLA/PBSL polymer blends obtained from static compressive testes

PLLA/PBSL	Young's modulus		Yield stress	
	[GPa]	Average value	[MPa]	Average value
100/0	2.90 3.49 3.52 2.39	3.07	108.0 105.9 99.4 99.2	103.1
90/10	3.02 3.91 6.73	4.55	88.0 88.8 93.3	90.0
80/20	2.83 4.21 4.56	3.87	75.7 82.6 80.7	79.7
70/30	1.91 3.66 4.15	3.24	67.5 74.3 76.5	72.8
0/100	0.50 0.45 0.47 0.41	0.46	43.2 39.7 41.0 36.0	40.0

Table 4 Fracture strain and tensile strength of PLLA/PBSL polymer blends obtained from static tensile testes

PLLA/PBSL	Fracture strain		Tensile strength	
		Average value	[MPa]	Average value
100/0	0.017	---	35.9	---
90/10	0.017 0.012	0.014	36.7 34.4	35.6
80/20	0.016 0.010	0.013	27.7 26.0	26.9
70/30	0.010 0.012	0.011	20.2 15.9	18.1
0/100	0.053	---	21.0	---

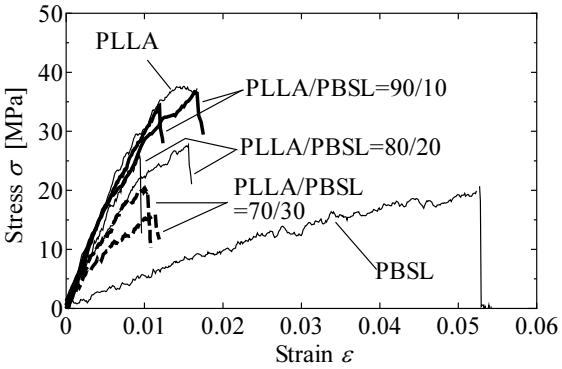

Fig. 8 Effect of PBSL content on tensile stress–strain curves at low strain rates (1×10^{-4} s^{-1})

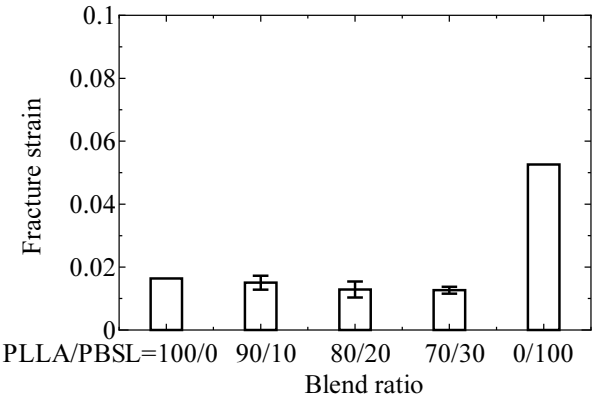

Fig. 9 Effect of PBSL content on fracture strain at low strain rates (1×10^{-4} s^{-1})

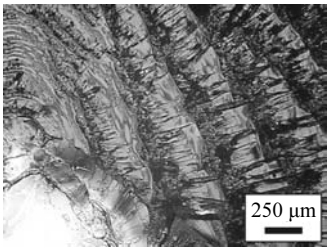

(a) PLLA/PBSL=100/0

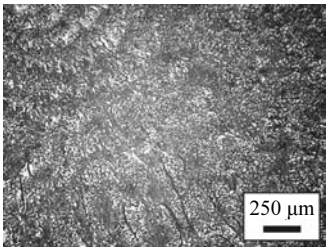

(b) PLLA/PBSL=90/10

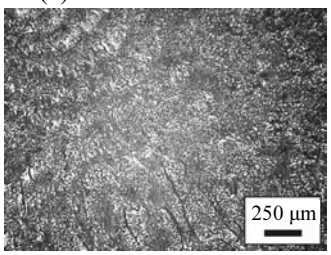

(c) PLLA/PBSL=80/20

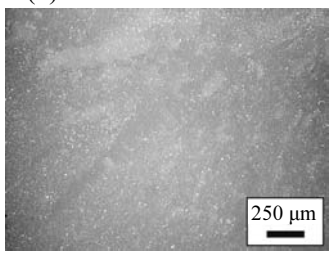

(d) PLLA/PBSL=70/30

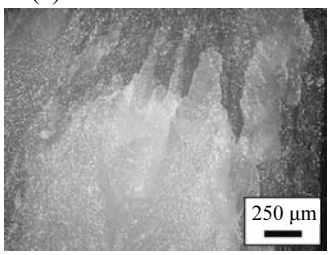

(e) PLLA/PBSL=0/100

Fig. 10 Microscope photographs of fracture surfaces after static tensile tests

Fig. 10 shows microscope photographs of the fracture surfaces after the static tensile tests using a digital microscope (Keyence Corporation, VH-Z75). A wave-like shape was clearly observed on the surface when PLLA/PBSL=100/0, and could be observed to some extent when PLLA/PBSL=90/10 and 80/20, whereas when PLLA/PBSL=70/30 and 0/100, a flat fracture surface was observed without any wave-like shape. We thought that this was the Mackerel pattern which has often been observed on fracture surfaces which is parallel and concentric craze strips (as observed in Fig. 11(a)). The Mackerel pattern disappeared when PBSL was increased. Fig. 11 shows enlarged images of Fig. 10 using SEM. When PLLA/PBSL=80/20 and 70/30, the fracture surfaces shown in Fig. 11 were almost the same as the cryo-fractured surfaces shown in Fig. 2. PBSL particles maintained a spherical shape and were not stretched. We can see many voids (vacant holes) when PLLA/PBSL= 70/30. It seems that, when PLLA/PBSL=80/20 and 70/30, a brittle fracture of the PLLA matrix occurred. In Fig. 110 (e), it can be clearly observed that, when PLLA/PBSL =0/100, ductile fracture with many stretch-zones appears.

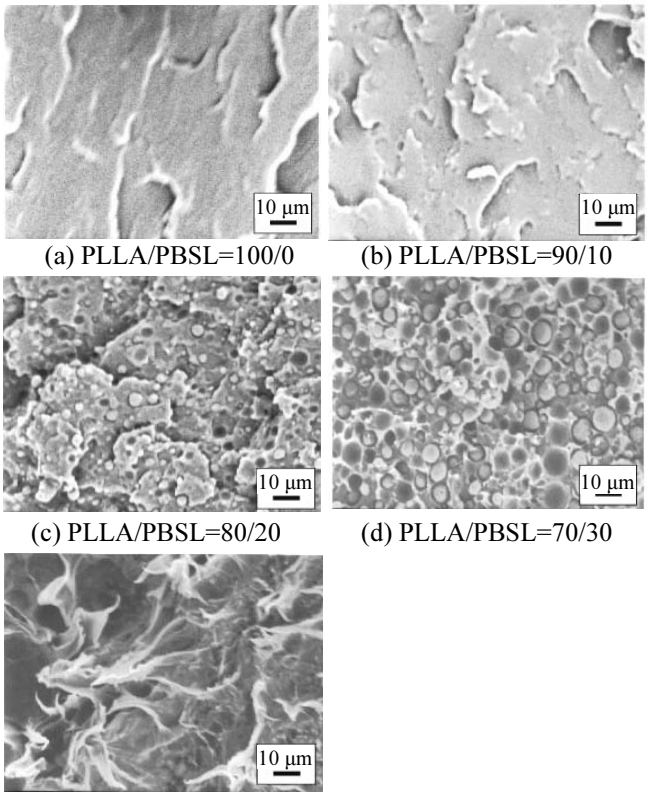

(a) PLLA/PBSL=100/0 (b) PLLA/PBSL=90/10

(c) PLLA/PBSL=80/20 (d) PLLA/PBSL=70/30

(e) PLLA/PBSL=0/100

Fig. 11 SEM images of fracture surfaces after static tensile tests

4.4 Dynamic tensile tests

Fig. 12 shows the nominal stress–nominal strain curves in the high strain rate region obtained by the tensile split Hopkinson bar method. Compared with Fig. 8, the fracture strain for high strain rate was slightly larger. The effect of strain rate was not large. Fig. 13 shows macroscopic photographs of the fracture surfaces after the dynamic tensile tests. Through-thickness direction is the vertical direction of photographs. Wave-like shapes were not observed on the surface and a flat fracture surface was observed when PLLA /PBSL=90/10, 80/20 and 70/30. We thought this was the mirror area which has often been observed on the fracture surface of brittle materials. Fig. 14 shows images of the fracture surfaces using SEM. The fracture surfaces shown in Fig. 14 were almost the same as the cryo-fractured surfaces shown in Fig. 2.

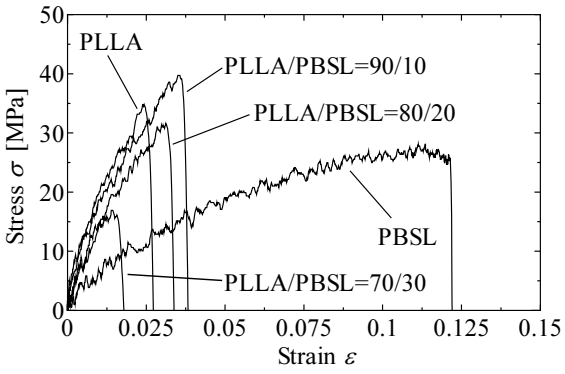

(a) Strain rates of 320 –350 s^{-1}

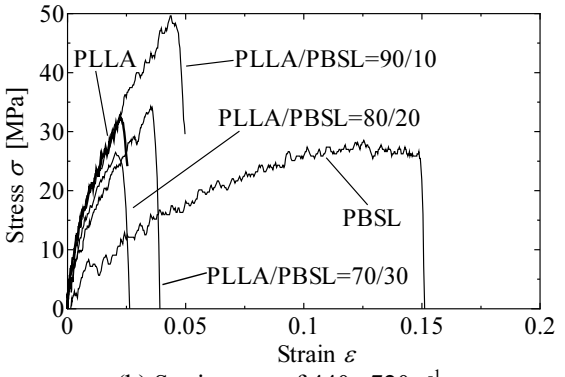

(b) Strain rates of 440 –720 s^{-1}

Fig. 12 Effect of PBSL content on tensile stress–strain curves at high strain rates

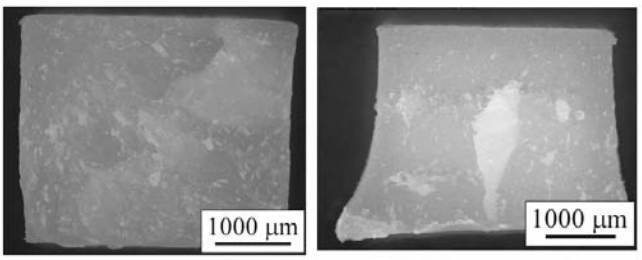

(a) PLLA/PBSL=90/10 (b) PLLA/PBSL=80/20

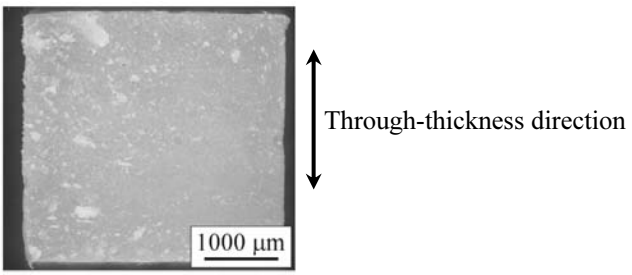

(c) PLLA/PBSL=70/30

Fig. 13 Macroscopic photographs of fracture surfaces after dynamic tensile tests

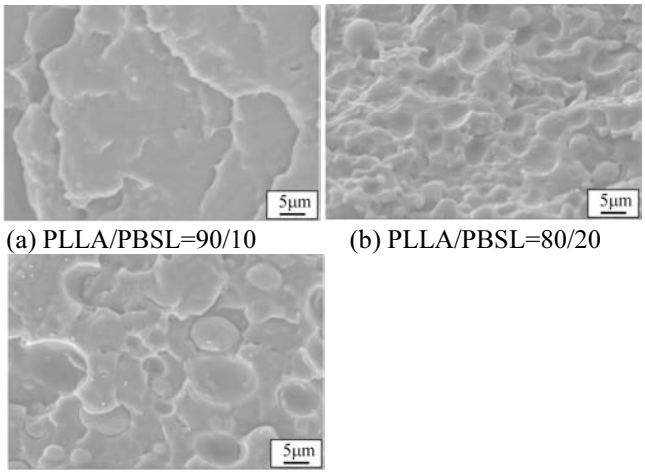

(a) PLLA/PBSL=90/10 (b) PLLA/PBSL=80/20

(c) PLLA/PBSL=70/30

Fig. 14 SEM images of fracture surfaces after dynamic tensile tests

4.5 Young's modulus and yield stress

Figs. 15(a) and (b) show the effect of PBSL content on the Young's modulus and yield stress at the low strain rates. The figures show the averaged values of Young's modulus and yield stress with the standard deviation. The standard deviation of Young's modulus was high when PLLA/PBSL=100/0 and 90/10. Predictably, the Young's modulus and yield stress of the polymer blends decreased gradually with increasing PBSL content. In the figure, the curves obtained from the Halpin-Tsai model [14], the Reuss model and the Voigt model [15] are also shown.

Halpin-Tsai model:

$$\frac{E}{E_m} = \frac{1+\xi\eta V_f}{1-\eta V_f} \tag{4}$$

$$\eta = \frac{\left(E_f / E_m\right)-1}{\left(E_f / E_m\right)+\xi}, \quad \xi = 2 \tag{5}$$

Reuss model:

$$\frac{1}{E} = \frac{V_f}{E_f} + \frac{V_m}{E_m} \tag{6}$$

Voigt model:

$$E = E_f V_f + E_m V_m \tag{7}$$

Here E is Young's modulus of the polymer blends, E_m is Young's modulus of the matrix, E_f is Young's modulus of the particles, V_m is the volume fraction of the matrix, and V_f is the volume fraction of the particles. In the case of the yield stress calculation, yield stresses σ_{max}, $\sigma_{max\text{-}m}$ and $\sigma_{max\text{-}f}$ were used instead of each Young's modulus. Because the densities of PLLA and PBSL are 1.26 g/cm^3 and 1.23 g/cm^3, the volume fractions of polymer blends were calculated from the mass fraction and are shown in Table 5. In Fig. 15(a), the curve of the Reuss model was located outside of the lower end of the results, while the line of the Voigt model was located outside of the upper end. The line of the Halpin-Tsai model was close to the tendency of the measured Young's modulus. In Fig. 14(b), the measured yield stresses were close to the curve of the Reuss model.

Table 5 Volume fraction of PLLA/PBSL blends

Mass fraction	Volume fraction
90 / 10	90.2 / 9.8
80 / 20	80.4 / 19.6
70 / 30	70.5 / 29.5

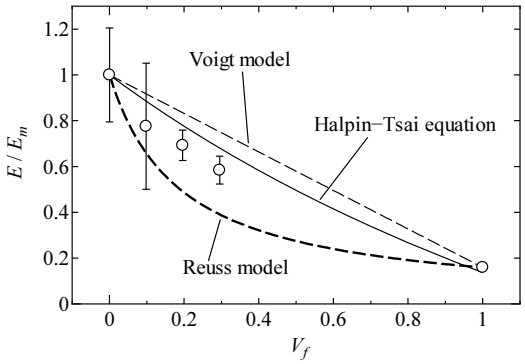

(a) Young's modulus

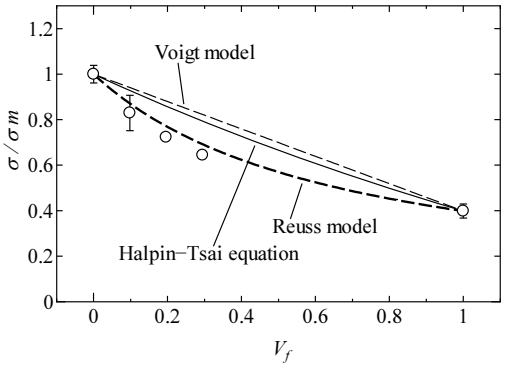

(b) Yield stress

Fig. 15 Young's modulus and yield stress from static compressive tests versus PBSL volume fraction

5. Conclusions

The PBSL content in the mixing ratios affected the stress–strain curves obtained for the PLLA/PBSL polymer blends. The yield stress of the blends in the compressive tests clearly decreased with increasing PBSL content, regardless of the strain rate. The PBSL content also affected the fracture surface from the static tensile tests. When PLLA/PBSL=100/0, 90/10 and 80/20, the Mackerel pattern was observed on the fracture surface from the static tensile tests. When PLLA/PBSL=70/30 and 0/100, the fracture surface from the static tensile tests was flat. Regardless of PBSL content, the fracture surface from of the dynamic tensile tests was flat. At low strain rates, the tendency of the Young's modulus and the yield stress of the polymer blends were close to those of the Halpin-Tsai model and Reuss model, respectively.

Acknowledgment

The authors are greatly indebted to Dr. K. Ogawa of the Space Dynamics Laboratory in Japan for his valuable advice with respect to the tensile split Hopkinson bar.

References

[1] Todo, M., Park, S.D., Takayama, S.D. and Arakawa, K.: Fracture Micromechanisms of Bioabsorbable PLLA/PCL Polymer Blends, *Engineering Fracture Mechanics*, **74** (2007), 1872-1883.

[2] Takayama, T., Todo, M. and Tsuji, H.: Effect of Annealing on the Mechanical Properties of PLA/PCL and PLA/PCL/LTI Polymer Blends, *Journal of the Mechanical Behavior of Biomedical Materials*, **4** (2011), 255-260.

[3] Harada, M., lida, K., Okamoto, K., Hayashi, H. and Hirano, K.: Reactive Compatibilization of Biodegradable Poly(lactic acid)/Poly(ε-caprolactone) Blends with Reactive Processing Agents, *Polymer Engineering & Science*, **48**-7 (2008), 1359–1368.

[4] Vilay, V., Mariatti, M., Ahmad, Z., Pasomsouk, K. and Todo, M.: Characterization of the Mechanical and Thermal Properties and Morphological Behavior of Biodegradable Poly(L-lactide)/Poly(ε-caprolactone) and Poly(L-lactide)/Poly(butylenes succinate-co-L-lactide) Polymer Blends, *Journal of Applied Polymer Science*, **114** (2009), 1784-1792.

[5] Harada, M. Ohya, T., Iida, K., Hayashi, H., Hirano, K. and Fukuda, H.: Increased Impact Strength of Biodegradable Poly(lactic acid)/Poly(butylene succinate) Blend Composites by Using Isocyanate as A Reactive Processing Agent, *Journal of Applied Polymer Science*, **106**-3 (2007), 1813–1820.

[6] Kobayashi, S. and Naito, K.: Degradation Properties of PLA/PBSU Polymer Blend Films, *Transactions of the Japan Society of Mechanical Engineers* A, **76**-771 (2010), 1514-1519. (in Japanese)

[7] Vannaladsaysy, V., Todo, M., Takayama, T., Jaafar, M., Zulkifli, A. and Pasomsouk, K.: Effect of Lysine Triisocyanate on the Mode I Fracture Behavior of Polymer Blend of Poly(L-lactic acid) and Poly (butylene succinate-co-L-lactide), *Journal of Materials Science*, **44**-11 (2009), 3006-3009.

[8] Umenaka, K., Koyama, K. and Sugimoto, M.: Rheological Properties of Poly (butylene succinate-co -lactate)/Poly (lactide) Blends, *Seikei- Kakou*, **23**-4 (2011), 229-234. (in Japanese)

[9] Vilay, V., Mariatti, M., Ahmad, Z., Pasomsouk, K. and Todo, M.: Improvement of Microstructure and Fractured Property of Poly(L-lactic acid) and Poly (butylene succinate-co-e-caprolactone) Blend Compatibilized with Lysine Triisocyanate, *Engineering Letters*, **18**-3 (2010), EL_18_3_13

[10] Nishida, M., Ichihara, H. and Fukuda, N.: Evaluation of Dynamic Compressive Properties of PLA/PBAT Polymer Alloys Using Split Hopkinson Pressure Bar, *Engineering Transactions*, **59**-1 (2011), 23–30.

[11] Gray, III G.T.: Classic Split Hopkinson Pressure Bar Testing, *ASM Handbook*, **8**, Mechanical Testing and Evaluation, ASM., (2000), 462-476.

[12] Chen, W. and Song, B.: *Split Hopkinson (Kolsky) Bar: Design, Testing and Applications*, Springer, 2010.

[13] Nakai, K. and Yokoyama, T.: Strain Rate Dependence of Compressive Stress-Strain Loops of Several Polymers, *J. of Solid Mechanics and Materials Engineering*, **2**-4, (2008), 557-566.

[14] Nielsen, L. E.: Morphology and the Elastic Modulus of Block Polymers and Polyblends, *Rheologica Acta*, **13**- 1 (1974), 86-92.

[15] Broutman, L. J. and Krock, R.H.: Modern Composite Materials, Addison Wesley, (1967).